

The Role of Magnetic Field Dissipation in the Black Hole Candidate Sgr A*

Robert F. Coker^{1*} and Fulvio Melia^{2*†}

^{*}Physics Department, The University of Arizona, Tucson, AZ 85721

[†]Steward Observatory, The University of Arizona, Tucson, AZ 85721

Received _____; accepted _____

¹NASA GSRP Fellow.

²Sir Thomas Lyle Fellow.

ABSTRACT

The compact, nonthermal radio source Sgr A* at the Galactic Center appears to be coincident with a $\sim 2.6 \times 10^6 M_\odot$ point-like object. Its energy source may be the release of gravitational energy as gas from the interstellar medium descends into its deep potential well. However, simple attempts at calculating the radiative spectrum and flux based on this picture have come tantalizingly close to the observations, yet have had difficulty in accounting for the unusually low efficiency in this source. Regardless of whether the radiating particles in the accretion flow are thermal or nonthermal, there now appear to be two principal reasons for this low conversion rate of dissipated energy into radiation: (1) the plasma separates into two temperatures, with the protons attaining a significantly higher temperature than that of the radiating electrons, and (2) the magnetic field \mathbf{B} is sub-equipartition, which reduces the magnetic bremsstrahlung emissivity, and therefore the overall power of Sgr A*. In this paper, we investigate the latter with a considerable improvement over what has been attempted before. In particular, rather than calculating \mathbf{B} based on some presumed model (e.g., equipartition with the thermal energy of the gas), we instead infer its distribution with radius empirically with the requirement that the resulting spectrum matches the observations. Our assumed ansatz for $\mathbf{B}(\mathbf{r})$ is motivated in part by earlier calculations of the expected magnetic dissipation rate due to reconnection in a compressed flow. We find reasonable agreement with the observed spectrum of Sgr A* as long as its distribution consists of 3 primary components: an outer equipartition field, a roughly constant field at intermediate radii ($\sim 10^3$ Schwarzschild radii), and an inner dynamo (more or less within the last stable orbit for a non-rotating black hole) which increases \mathbf{B} to about 100 Gauss. The latter component accounts very well for the observed

sub-millimeter hump in this source.

Subject headings: accretion—black hole physics—hydrodynamics—Galaxy:
center—magnetic fields—magnetohydrodynamics—plasmas—turbulence

1. Introduction

The Galactic center (GC) has long been suspected of harboring a central mass concentration, which appears to be coincident with the unique, nonthermal radio source, Sgr A*. Haller et al. (1996) used the velocity dispersions of stars at $\gtrsim 0.1$ pc from Sgr A* to derive a compact mass of $\sim 2 \times 10^6 M_\odot$. This is consistent with the value of $\sim 2.5 - 3.2 \times 10^6 M_\odot$ derived more recently by Genzel et al. (1996), using the radial velocities and velocity dispersions of ~ 25 early-type stars and of ~ 200 red giants and supergiants within the central 2 pc. A third technique for tracing the central gravitational potential is based on the acquisition of proper motions for the $\sim 50 - 100$ brightest stars within the radial range $\sim 0.004 - 0.4$ pc (Eckart & Genzel 1996; Ghez et al. 1998). These stellar motions seem to require a central dark mass of $(2.6 \pm 0.2) \times 10^6 M_\odot$, in good agreement with earlier ionized gas kinematics and the velocity dispersion measurements.

Of course, showing that the GC must contain a centralized mass concentration does not necessarily imply that this dark matter is in the form of a compact object with a few million solar masses. It does not even imply that the unusual radio source Sgr A* must be associated with it. VLBA images of Sgr A* with milliarcsecond resolution (Bower & Backer 1998) show that at $\lambda 7$ mm, its size is 0.76 ± 0.04 mas, or roughly 6.2×10^{13} cm, much smaller than ~ 0.01 pc, the present limiting region within which the $2 - 3 \times 10^6 M_\odot$ are contained. So the dark matter may be distributed, perhaps in the form of white dwarfs, neutron stars, or $\sim 10 M_\odot$ black holes (e.g., Haller et al. 1996), though the latest stellar kinematic results appear to rule out the first two possible constituents (Genzel et al. 1996).

Whatever the composition of a distributed mass concentration is, one is left with the task of accounting for the nature of Sgr A* itself. It is likely that many of Sgr A*'s characteristics are associated with the liberation of gravitational energy as gas from the ambient medium falls into a central potential well (Melia 1994; see also Ozernoy 1989 for an

alternative conclusion regarding wind accretion). There is ample observational evidence in this region for the existence of rather strong winds in and around Sgr A* itself (from which the latter is accreting), e.g., the cluster of mass-losing, blue, luminous stars comprising the IRS 16 assemblage located within several arcseconds from the nucleus. Measurements of high outflow velocities associated with IR sources in Sgr A West (Krabbe et al. 1991) and in IRS 16 (Geballe et al. 1991), the H_2 emission in the circumnuclear disk (CND) from molecular gas being shocked by a nuclear mass outflow (Genzel et al. 1996; but see Jackson et al. 1993 for the potential importance of UV photodissociation in promoting this H_2 emission), broad $\text{Br}\alpha$, $\text{Br}\gamma$ and He I emission lines from the vicinity of IRS 16 (Hall et al. 1982; Allen et al. 1990; Geballe et al. 1991), and radio continuum observations of IRS 7 (Yusef-Zadeh & Melia 1991), provide clear evidence of a hypersonic wind, with a velocity $v_w \sim 500 - 1000 \text{ km s}^{-1}$, a number density $n_w \sim 10^{3-4} \text{ cm}^{-3}$, and a total mass loss rate $\dot{M}_w \sim \times 10^{(-3)-(-4)} \dot{M}_\odot$, pervading the inner parsec of the Galaxy. Even so, the observations do not yet provide sufficient information for us to identify the physics of accretion when the infalling gas penetrates to within about 10^3 or 10^4 Schwarzschild radii of the central object.

1.1. Behavior of the Accreting Gas at Small Radii

Three-dimensional hydrodynamic simulations (Coker & Melia 1997) indicate that the accreted specific angular momentum λ (in units of cr_s , where $r_s \equiv 2GM/c^2$ is the Schwarzschild radius in terms of the black hole mass M) can vary by 50% over $\lesssim 200$ years with an average equilibrium value for λ of 40 ± 10 . Thus, even with a possibly large amount of angular momentum present in the wind, relatively little specific angular momentum is accreted. This is understandable since clumps of gas with a high specific angular momentum do not penetrate to within $1 R_A$, where

$$R_A \equiv 2GM/v_w^2 \tag{1}$$

is the capture radius defined in terms of the wind velocity v_w at infinity. The variability in the sign of the components of λ suggests that if an accretion disk forms at all, it dissolves, and reforms (perhaps) with an opposite sense of spin on a time scale of ~ 100 years.

The captured gas is highly ionized and magnetized, so it radiates via bremsstrahlung, cyclo-synchrotron and inverse Compton processes. However, for purely spherical accretion, the efficiency of converting gravitational energy into radiation is quite small (as little as 10^{-4} in some cases), so most of the dissipated energy is carried inwards (Shapiro 1973; Ipser & Price 1977; Melia 1992). In fact, if the magnetic field is a negligible fraction of its equipartition value (see below), Sgr A* would be undetectable at any frequency, except perhaps at soft X-ray energies. But as the plasma continues to compress and fall toward smaller radii, one or more additional things can happen, each of which corresponds to a different theoretical assumption, and therefore a potentially different interpretation.

The questions one may ask include the following: (1) Does the flow carry a large specific angular momentum so that it forms a disk with lots of additional dissipation? (2) Does the flow produce a radiatively dominant non-thermal particle distribution at small radii (e.g., from shock acceleration), or does thermal emission continue to dominate the spectrum? (3) Does the flow lead to an expulsion of plasma at small radii that forms a non-thermal jet, which itself may then dominate the spectrum? These, either individually or in combination, have led to a variance of assumptions about the nature of the inflowing gas that then form the basis for the development of different interpretations.

Observationally, a key issue is why the infalling gas maintains a low radiative efficiency. Beckert & Duschl (1997) suggest that shocks in the accreting plasma produce a power-law electron distribution, which is truncated by strong cooling. This forms a “quasi” mono-energetic distribution. The overall emission, which is strictly non-thermal, is suppressed by constraining the number density of relativistic particles and the intensity of

the magnetic field (at about 5 to 10 Gauss).

Falcke, Mannheim and Biermann (1993) and Falcke & Biermann (1999), on the other hand, assume that the infalling plasma eventually produces a jet of power-law electrons whose number density varies with radius in the expulsion. The overall emission, which is a sum of non-thermal components, is also suppressed by constraining the particle number density and hence the equipartition magnetic field, both of which are assumed to be scaled by a low luminosity disk.

In the picture developed by Narayan, et al. (1998), the infalling gas is assumed to carry a very large angular momentum, so that a disk forms with an outer radius at more than 10^5 Schwarzschild radii. To suppress the overall emission, which now includes the additional dissipation of this large angular momentum, it is also assumed that the electron temperature is much lower than that of the protons ($T_e \ll T_p$). In fact, $T_e < 10^{10}$ K. Since the electrons do the radiating, the efficiency remains small even though the protons are very hot.

1.2. A Sub-equipartition Magnetic Field

The idea that Sgr A*’s low radiating efficiency is due to a sub-equipartition magnetic field B deserves further attention, especially in view of the fact that the actual value of B depends strongly on the mechanism of field line annihilation, which is poorly understood. Two processes that have been proposed are (i) the Petschek (1964) mechanism, in which dissipation of the sheared magnetic field occurs in the form of shock waves surrounding special neutral points in the current sheets and thus, nearly all the dissipated magnetic energy is converted into the magnetic energy carried by the emergent shocks; and (ii) van Hoven’s (1979) tearing mode instability, which relies on resistive diffusion of the magnetic

field and is very sensitive to the physical state of the gas. In either case, the magnetic field dissipation rate is a strong function of the gas temperature and density, so that assuming a fixed ratio of the magnetic field to its equipartition value may not be appropriate.

Kowalenko & Melia (1999) have used the van Hoven prescription to calculate the magnetic field annihilation rate in a cube of ionized gas being compressed at a rate commensurate with that expected for free-fall velocity onto the nucleus at the Galactic Center. Whereas the rate of increase $\partial B/\partial t|_f$ in B due to flux conservation depends only on the rate \dot{r} of the gas, the dissipation rate $\partial B/\partial t|_d$ is a function of the state variables and it is therefore not necessarily correlated with \dot{r} . Although these attempts at developing a physical model for magnetic field dissipation in converging flows is still rather simplistic, it is apparent from the test simulations that the equipartition assumption is not always a good approximation to the actual state of a magnetohydrodynamic flow, and very importantly, that the violation of equipartition can vary in degree from large to small radii, in either direction. As such, calculations that assume equipartition of the magnetic field with the gas throughout the domain of solution may be greatly underestimating the importance of the deviations of B from its B_{eq} value since the predicted spectrum relies critically on the contribution from magnetic bremsstrahlung.

1.3. Impact on Sgr A*’s Spectrum

The first serious attempt at modeling the spectrum of Sgr A* as being due to emission by the accreting gas was carried out by Melia (1992, 1994), who assumed a black hole mass of $\approx 10^6 M_\odot$. But this mass is no longer consistent with the now more accurately known value of $\sim 2.6 \times 10^6 M_\odot$, which accounts for a factor of ~ 7 increase in \dot{M} . In addition, the earlier calculations integrated the cyclo-synchrotron emissivity out to the lowest 20 harmonics only, which misses some of the contribution to the flux by the highest

temperature gas at the smallest radii (Mahadevan, Narayan & Yi 1996). In this paper, we recalculate the spectrum produced by a quasi-spherical infall onto Sgr A* using the updated mass value, a more accurate handling of the magnetic bremsstrahlung and an empirical fit to the magnetic field, motivated by the simulations of magnetic dissipation discussed above. In section § 2, we derive the equations governing this spherical infall, which we adopt as a simplified version of the real accretion picture. Of course, the real accretion flow will deviate from radial at small distances from the black hole, where the gas begins to circularize with its advected specific angular momentum. In a fully self-consistent calculation, we will use the distributions derived from an actual 3D hydrodynamic simulation as the basis for calculating the emissivity. The model parameters and results of our calculations are discussed in § 3, and we summarize our conclusions in § 4.

2. Equations Governing Spherical Accretion

2.1. The Radial Profiles

We follow the sequence of derivations in Shapiro (1973), with the primary differences being the inclusion of the magnetic field and a radiation pressure term and the fact that we restrict our attention to supersonic flows. The equation of mass conservation reduces to

$$\dot{M} = 4\pi r^2 \rho v , \quad (2)$$

where \dot{M} is the mass accretion rate onto the black hole, ρ is the mass density of the accreting gas, $-v \equiv u^r$ is the radial component of the fluid 4-velocity (but defined to be positive inwards, so that $v = -dr/d\tau$ for the infalling plasma), and r is the distance from the black hole. Equation (2) can be recast into the form

$$\frac{n'}{n} = - \left(\frac{v'}{v} + \frac{2}{r} \right) , \quad (3)$$

where a prime denotes d/dr . At R_0 , where the numerical integration begins, we assume that the gas is non-relativistic and that the gravitational potential is weak.

The second equation, arising from momentum conservation, is the steady state relativistic Euler equation for a spherical geometry:

$$vv' = - \left(\frac{c^2 + v^2 - 2GM/r}{P + e_\rho + \epsilon} \right) P'_{th} - \frac{GM}{r^2} , \quad (4)$$

where the mass of the central black hole is given by M , the total pressure is given by

$$P = \frac{B^2}{8\pi} + P_{th} , \quad (5)$$

the non-magnetic pressure is given by

$$P_{th} = 2nkT + P_{rad} , \quad (6)$$

the particle mass-energy density is

$$e_\rho = m_p c^2 n , \quad (7)$$

and the internal energy density of the gas is

$$\epsilon = \alpha nkT + 3P_{rad} + \frac{B^2}{8\pi} . \quad (8)$$

In the fully ionized but non-relativistic limit (i.e., $10^5 < T < 6 \times 10^9$ K), $\alpha = 3$. On the other hand, in the relativistic electron limit ($6 \times 10^9 < T < 10^{13}$ K), $\alpha = 9/2$. We use the general expression from Chandrasekhar (1939) that is valid for all T :

$$\alpha = 3 + x \left(\frac{3 K_3(x) + K_1(x)}{4 K_2(x)} - 1 \right) + y \left(\frac{3 K_3(y) + K_1(y)}{4 K_2(y)} - 1 \right) , \quad (9)$$

where $x \equiv m_e c^2 / kT$, $y \equiv m_p c^2 / kT$ and K_i refers to the i^{th} order modified Bessel function.

We assume that the gas consists solely of completely ionized hydrogen. Note that since we will assume a mostly radial B (see below), the numerator of Equation (4) does not

depend on the magnetic field. That is, there is no large scale current, since $\mathbf{v} \times \mathbf{B} = \mathbf{0}$. The radiation pressure, P_{rad} , is given by the Rayleigh-Jeans approximation

$$P_{rad} = \frac{8\pi}{9} kT \left(\frac{\nu_m}{c} \right)^3, \quad (10)$$

where ν_m is the frequency below which the radiative emission is highly absorbed, so that the optical depth, $\tau_r^\infty(\nu_m)$, from r to infinity is unity. This assumes that the accretion flow is relatively unimpeded by radiation pressure, or, in other words, that the accretion is sub-Eddington. As mentioned in Melia (1992), with $L_{SgrA*} \sim 10^5 L_\odot \ll L_{Ed} \sim 10^{11} L_\odot$, (Zylka et al. 1995; Shapiro and Teukolsky 1983), this certainly appears to be the case for Sgr A*. Numerically, this means that $h\nu_m \ll kT$, which we verify *a posteriori*.

The third primary equation follows from energy conservation, which we derive from the first law of thermodynamics:

$$\frac{d}{d\tau} \left(\frac{e_\rho + \epsilon}{n} \right) = -P_{th} \frac{d}{d\tau} \left(\frac{1}{n} \right) + \frac{\Gamma - \Lambda}{n}, \quad (11)$$

where τ is the proper time in the gas frame. The use of P_{th} rather than P assumes that the compression of the gas is parallel to the magnetic field lines (i.e., radial inflow with a mostly radial B). The heating (Γ) and cooling (Λ) terms render the flow non-adiabatic (i.e., $ds/d\tau \neq 0$). The radiative cooling includes magnetic bremsstrahlung and electron-ion and electron-electron thermal bremsstrahlung (see Melia 1994, with an updated prescription in Melia & Coker 1999). Local UV heating from nearby stars results in a minimum gas temperature of 10^{4-5} K (Tamblyn et al. 1996), but the shocked gas at the model's outer radius, R_0 , is expected to be hotter. Thus, the major heating term (other than the effects of compression) is expected to be due to magnetic field reconnection. Specifically, we use (see Ipser & Price 1982)

$$\Gamma = \frac{nv}{8\pi} \left\{ \left(\frac{B^2}{n} \right)' - \frac{B^2}{n} \left(\frac{v'}{v} - \frac{2}{r} \right) \right\}. \quad (12)$$

Thus, if the magnetic field is flux conserved, for which $B(r) \propto r^{-2}$, then no reconnection is taking place and $\Gamma = 0$. However, if the magnetic field remains in approximate kinetic equipartition with the gas, meaning that its pressure increases in tandem with the ram pressure of the accreting gas ($P_{mag}/P_{ram} \sim \text{constant}$), then $B(r) \propto r^{-5/4}$, and $\Gamma \neq 0$. Since $T(r)$, $v(r)$, and $n(r)$ will turn out not to be perfect power-laws, these statements are only approximate.

To find the velocity gradient, v' , we place the above definitions for P_{th} and P_{rad} into Equation (4) to get

$$vv' = - \left(\frac{c^2 + v^2 - 2GM/r}{P + e_\rho + \epsilon} \right) \left(2k[n'T + nT'] + \frac{8k\pi}{9c^3} [T'\nu_m^3 + T3\nu_m^2\nu'_m] \right) - \frac{GM}{r^2}. \quad (13)$$

Thus, substituting for n' from Equation (3), we have,

$$v' = \frac{-Hv [2nk(T' - 2T/r) + (8k\pi/9c^3)(T'\nu_m^3 + T3\nu_m^2\nu'_m)] - vGM/r^2}{v^2 - 2nkTH}, \quad (14)$$

where, for ease of writing, we have defined the quantity

$$H \equiv \frac{c^2 + v^2 - 2GM/r}{P + e_\rho + \epsilon}. \quad (15)$$

Note that in the non-relativistic and small B limit, $H = 1/\rho$. For simplicity, we write v' as the sum of two terms:

$$v' = fT' + g, \quad (16)$$

where

$$f \equiv \frac{-Hvk(2n + 8\pi\nu_m^3/9c^3)}{v^2 - 2nkTH}, \quad (17)$$

and

$$g \equiv \frac{-HvkT(-4n/r + 8\pi\nu_m^2\nu'_m/3c^3) - vGM/r^2}{v^2 - 2nkTH}. \quad (18)$$

The form of these expressions is that of the classic wind equations (see, Parker 1960; Melia 1988). In the simulations we consider here, the gas is supersonic at R_0 and remains

supersonic on its inward trajectory (i.e., for $r < R_0$). We, therefore, avoid the special handling required for solutions that cross any sonic points, where the denominator of Equation (14) vanishes.

Since $d(e_\rho/n)/d\tau = 0$, Equation (11) reduces to

$$\frac{d}{d\tau} \left(\frac{\epsilon}{n} \right) = -P_{th} \frac{d}{d\tau} \left(\frac{1}{n} \right) + \frac{\Gamma - \Lambda}{n} . \quad (19)$$

Substituting in P_{th} and ϵ , we get

$$-v \frac{d}{dr} \left(\alpha k T + \frac{8\pi\nu_m^3 k T}{3nc^3} + \frac{B^2}{8\pi n} \right) = -v \left(-2nkT - \frac{8\pi\nu_m^3 k T}{9c^3} \right) \frac{-n'}{n^2} + \frac{\Gamma - \Lambda}{n} . \quad (20)$$

Substituting in Equation (3) and explicitly taking the derivatives, we then obtain

$$\begin{aligned} T' \left(\alpha k + \frac{8\pi\nu_m^3 k}{3nc^3} \right) = & - \left(\frac{v'}{v} + \frac{2}{r} \right) \left(2kT + \frac{32\pi\nu_m^3 k T}{9nc^3} + \frac{B^2}{8\pi n} \right) \\ & + \frac{\Lambda - \Gamma}{nv} - \frac{BB'}{4\pi n} - \frac{8\pi\nu_m^2 k T \nu_m'}{nc^3} . \end{aligned} \quad (21)$$

We use Equations (14) and (21) to determine v' and T' , respectively, then solve for v and T using an implicit differencing scheme, with

$$T_{j+1} = T_j + (r_{j+1} - r_j) T'_{j+1} , \quad (22)$$

where T'_{j+1} is a function of T_j, v_j, r_j, B_j , and v'_j . Similar relations hold for v . Thus, the whole flow is determined given some outer boundary conditions (R_0, β, f_v , and f_T ; see below), the empirically inferred behaviour of $B(r)$, and a prescription for finding ν_m . Note that boundary condition values for T', v', B' , and ν'_m are also needed; at the outer boundary, we assume the flow is optically thin, in adiabatic free-fall with a thermal equipartition field and determine the derivatives accordingly.

2.2. The Optical Depth and a Prescription for ν_m

Since the gas is not expected to be optically thin at low radio frequencies, the effective optical depth as a function of frequency must be determined before the radial profiles can be calculated. For Sgr A*, we assume (and check *a posteriori*) that the energy absorbed at any given radius is small compared to the thermal and kinetic energy at that radius; this is not likely to be true for objects that are accreting closer to their Eddington luminosity. Further, we assume that multiple scatterings are unimportant.

Following Rybicki & Lightman (1979), we use, for an effective optical depth in a zone of observed size $dr_0 (= r_{j+1} - r_j)$ at infinity,

$$\tau_j = Cdr\sqrt{\alpha_{abs}(\alpha_{abs} + n\sigma_{scat})}, \quad (23)$$

where

$$dr = dr_0 \frac{1 - \beta\bar{\mu}}{\sqrt{(1 - 2GM/rc^2)(1 - \beta^2)}}, \quad (24)$$

α_{abs} is the absorption coefficient, n is the electron number density, and σ_{scat} is the electron scattering cross section. Note that $r_{j=1} = 1r_s = 2GM/c^2$. The coefficient C in Equation (23) is a geometric term arising from the fact that in spherical symmetry, the average path length of a photon that reaches the observer is somewhat larger than dr_0 . It is given by

$$C = \min\left\{\frac{1 + \sqrt{3}}{2}, \frac{2}{1 - \mu_{max}}\right\}, \quad (25)$$

where μ_{max} is defined in Equation (27). In Equation (24),

$$\beta = \frac{v}{c\sqrt{1 + (v/c)^2 - 2GM/rc^2}} \quad (26)$$

and $\bar{\mu}$ is the average of the minimum of the cosine of the angle between the line of sight and the flow (which is here -1) and the maximum,

$$|\mu^{max}| = \sqrt{\frac{27}{4} \left(\frac{2GM}{rc^2}\right)^2 \left(\frac{2GM}{rc^2} - 1\right) + 1}, \quad (27)$$

given by Zeldovich & Novikov (1971). This maximum in μ is a consequence of the fact that not all of the emitted photons reach the observer; some are captured by the black hole. Note that μ_{max} changes sign and becomes negative at radii smaller than $1.5 r_s$. Also, $\mu_{max} \rightarrow -1$ at the event horizon since the curvature in the trajectory of photons emitted at other angles takes them back into the event horizon. Although τ has a more complex angular dependence, the use of $\bar{\mu}$ in Equation (24) is a necessary simplification at this point.

For α_{abs} , we use Kirchoff's Law,

$$\alpha_{abs} = j_\nu / B_\nu , \quad (28)$$

where j_ν is the total emissivity (in $\text{ergs cm}^{-3} \text{ s}^{-1} \text{ Hz}^{-1} \text{ steradian}^{-1}$) and B_ν is the blackbody Planck function. For the models discussed here, we use a total emissivity that includes cyclo-synchrotron emission (Coker & Melia 1999) and electron-ion and electron-electron bremsstrahlung (Melia & Coker 1999). For σ_{scat} we use the exact scattering cross section (see, e.g., Lang 1980)

$$\sigma_{scat} = \frac{3}{4} \sigma_T \left[\frac{1+x}{x^3} \left(\frac{2x(1+x)}{1+2x} - \ln(1+2x) \right) + \frac{1}{2x} \ln(1+2x) - \frac{1+3x}{(1+2x)^2} \right] , \quad (29)$$

where $x = \gamma h\nu / (mc^2)$ and

$$\gamma = \max\{1, \sqrt{12}kT/mc^2\} \quad (30)$$

is the RMS value of the thermal velocity at the temperature in the given zone.

Finally, to find the total optical depth from zone j out to infinity at some observed frequency ν_0 , related to the emitted frequency ν by

$$\nu_0 = \nu \frac{\sqrt{(1 - 2GM/rc^2)(1 - \beta^2)}}{1 - \beta\bar{\mu}} , \quad (31)$$

we use

$$\tau_{\nu_0}^\infty = \sum_{k=j+1}^{k=\infty} (r_j/r_k)^2 \tau_k . \quad (32)$$

The minimum frequency ν_m that a photon needs to have in order to escape is found by iteratively determining the wavelength at which τ_k is unity with the caveat that ν_m not be less than the plasma frequency

$$\nu_p = e \sqrt{\frac{n}{\pi m_e}} . \quad (33)$$

This caveat is required since photons with a frequency less than ν_p are unable to propagate and are thus trapped by the infalling gas. Once the radial profiles (optical depth, density, velocity, and temperature) are determined, it is possible to calculate the emission spectrum for a given magnetic field profile.

2.3. Calculation of the Spectrum

Now we are ready to calculate the predicted observable luminosity L_{ν_0} at infinity (see Shapiro 1973; Ipser & Price 1982; and applied to Sgr A* in Melia 1992, 1994):

$$L_{\nu_0} = 8\pi^2 \sum_{j=1}^{j=J} e^{-\tau_{\nu_0}^\infty(j)} r_j^2 (1 - \beta^2) \int_{-1}^{\mu_{max}} \frac{d\mu}{(1 - \beta\mu)^2} I_\nu , \quad (34)$$

where, if the emitting zone is optically thick (i.e., if $\tau_j > 1$), then

$$I_\nu = B_\nu (1 - e^{-\tau_j}) . \quad (35)$$

Otherwise

$$I_\nu = j_\nu e^{-\tau_j} dr . \quad (36)$$

In these two expressions, B_ν and j_ν depend on μ not $\bar{\mu}$. The use of τ_j here is a calculational simplification; ideally, it too should be a function of μ . The sum over j is truncated at J , for which $r_J \equiv R_0$. It is assumed that $\tau_{\nu_0}^\infty(J) = 0$. This ignores the possible absorption by Sgr A West of the low frequency ($\nu_0 < 10^9$ Hz) radiation (Beckert et al. 1996). Sgr A West is an HII region surrounding Sgr A*.

3. Parameters for a Spherical Accretion Model for Sgr A*

The stellar winds that accrete onto Sgr A* are thought to be hypermagnetosonic, so it is sensible to continue using the standard definition of an accretion radius (Eq. [1]), which is defined to be the point at which the gravitational potential energy is equal to the *initial* kinetic energy of the gas, but using an average of the stellar wind velocities weighted by the mass loss rate. For the Galactic Center, $R_A \sim 10^{16-17}$ cm. However, this definition of R_A does not necessarily give the physical radius at which the capture always occurs. For example, wind-wind collisions, combined with radiative cooling, can reduce the effective value of v_w . For simplicity, we use this standard definition of R_A to set the primary length scale of the problem, and put $R_0 = f_R R_A$, where f_R is a parameter of order unity.

Now, \dot{M} is likely to be a fraction of the total GC wind, \dot{M}_w , which is estimated to be $\sim 3 \times 10^{-3} M_\odot \text{ yr}^{-1}$ (Geballe et al. 1991). However, more recent work suggests that the mass loss rate of at least some of the central massive stars is less than previously thought (Hanson et al. 1998), so that \dot{M}_w may be smaller as well. If the GC wind is dominated by a source some distance $D > R_A$ away from Sgr A*, then one would expect

$$\dot{M} = \frac{R_A^2 \dot{M}_w}{D^2} = \frac{(2GM)^2 \dot{M}_w}{v_w^4 D^2}. \quad (37)$$

For example, if the 1000 km s^{-1} wind from IRS 13E1 (which is thought to be ~ 0.16 pc away from Sgr A*; see Melia & Coker 1999), dominates the flow, then $\dot{M} \sim 10^{21} \text{ g s}^{-1}$. Observationally, the mass accretion rate is not very well constrained; a reasonable range is $\sim 10^{20-22} \text{ g s}^{-1}$. For all of the models presented here, we assume that the mass M of the central black hole is $2.6 \times 10^6 M_\odot$, based on the latest observations (Eckart & Genzel 1999; Ghez et al., 1998). The magnetic field B_0 at $1 R_A$ is thought to be a few milliGauss (Yusef-Zadeh et al. 1996) but its large scale average value may be a few times smaller than this (Marshall et al. 1995). In practice, we use a value for B_0 such that at R_0 the magnetic

field is close to thermal equipartition:

$$B^2/8\pi = P_{mag} = \eta P_{thermal} = \eta 2nkT, \quad (38)$$

where η is a parameter of order unity. Together, \dot{M} and η effectively determine the normalization of the model spectrum.

From a combination of HeI line observations (Najarro et al. 1997) and hydrodynamic modeling (Coker & Melia 1997), the accreting wind is thought to be supersonic at R_0 with a temperature $T_0 \sim 10^6$ – 10^7 K and a velocity $v_0 \sim 10^2$ – 10^3 km s $^{-1}$. The temperature, T_w , and velocity, v_w , of the individual stellar winds that accrete onto Sgr A* are not necessarily the same as T_0 and v_0 . Wind-wind shocks and subsequent radiative cooling and acceleration result in $T_0 \gtrsim T_w$ and $v_0 \lesssim v_w$. The winds, which originate well outside of $1 R_A$, are originally hypersonic with a Mach number of 10-30, but by the time they reach $1 R_A$, they are on average only mildly supersonic with a Mach number of 1-3. The non-zero velocity at infinity tends to make $v_0 > v_{ff}$, where v_{ff} is the free-fall velocity, while shocks tend to have the opposite effect, making $v_0 \sim v_{ff}/4$. Therefore, for simplicity, we assume that v_0 is given by a fraction f_v , of order unity, of the free-fall value. With $R_0 = f_R R_A$ and Equation (1), we then have

$$v_0 = f_v v_w = f_v \sqrt{\frac{2GMf_R}{R_0}}. \quad (39)$$

In order to end up with a supersonic accretion solution, it is also necessary to set T_0 to be less than the local virial temperature, i.e.,

$$\frac{2kT_0}{m_p} < \frac{GM}{2R_0} \equiv \frac{2kT_{vir}}{m_p}. \quad (40)$$

We parameterize the starting temperature according to the prescription $T_0 = f_T T_{vir}$, where again f_T is of order unity.

3.1. Angular Momentum Considerations

Some accretion models of Sgr A* (e.g., Narayan et al. 1995) assume that $v_0 \ll v_{ff}$, requiring a deceleration mechanism fairly close to $1 R_A$. Since T_0 and B_0 are too small to decelerate the inflowing gas, the most likely reason for v_0 being so small would probably be that the gas contains a greater specific angular momentum than is seen in the hydrodynamic simulations (Ruffert & Melia 1994; Coker & Melia 1997). With the wind originating from more than a dozen sources distributed fairly isotropically around Sgr A* (Melia & Coker 1999), the time averaged specific angular momentum accreted by the black hole is likely to be small. This is the conclusion to which one is led with the current series of hydrodynamic simulations. The circularization radius at which the accreted specific angular momentum is equal to its Keplerian value is

$$R_{circ} = 2\lambda^2 r_s, \quad (41)$$

where $r_s \equiv 2GM/c^2$ is the Schwarzschild radius and λ is the accreted specific angular momentum in units of cr_s . The hydrodynamic simulations suggest that λ is highly time variable with a value in the range 2 – 50. However, these calculations have had limited physical resolution near the black hole and they have therefore sampled the λ accreted within the region $R_{boundary} \gg r_s$. As one would expect, tests have shown that smaller values of $R_{boundary}$ result in smaller values of λ carried across that threshold. Thus, the average values for λ given above may be thought of as upper limits so that $R_{circ} \ll R_A$. Similarly, the viscous transport of angular momentum outward and a possible mass loss via a wind off the disk (see, e.g., Xu & Chen 1997) should result in $\dot{M}(R_{circ}) > \dot{M}(r_s)$. Numerical calculations as yet do not have the physical resolution to verify this in the case of Sgr A*.

More importantly, these simulations indicate that the vector *direction* of the accreted specific angular momentum is highly time variable and dependent on conditions outside of the accretion radius, with sign changes occurring on a time scale of 1-50 years. Thus,

with R_{circ} representing the length scale within the nascent disk (though the distribution of angular momentum outwards may increase the disk’s outer radius somewhat above this value), even if such a disk forms, it is not likely to be stable over a time scale of more than a few decades, since the gas contains no long term preferred angular momentum axis. Recent work (Genzel 1998) suggests that the wind sources may have a small net rotation around Sgr A* and, if the resulting additional angular momentum is not canceled in wind-wind collisions, then angular momentum could play a more significant role in the spectrum of Sgr A* than we assume here.

3.2. The Magnetic Field

In this paper, we do not attempt (as Kowalenko & Melia 1999 did) to determine the magnetic dissipation rate from first principles, but rather we will use our fits to the observed spectrum of Sgr A* to infer empirically what the profile of B should be in order to validate this picture. In other words, we have a sense of how B might behave (most likely different from simple equipartition) based on the calculations of Kowalenko & Melia (1999), and we use that algorithm for $B(r)$ to fit the spectrum. We find that a 3 component profile is necessary and sufficient for this purpose. The profile of B affects primarily the heating term, Γ , and the magnetic bremsstrahlung emissivity, j_ν^{sync} , as discussed above. With 3 components, we have 5 parameters describing the magnetic field: 3 power-law indices (p_1, p_2, p_3) and the location of 2 breakpoints (r_1, r_2). Since the magnetic field of the ISM is observed to be approximately in thermal equipartition, we fix the first index, p_1 , so that $B(r) \propto r^{-5/4}$, or $P_{mag} = \eta P_{ram}$. The shape of the final spectrum is sensitive to the remaining 4 parameters (r_1, p_2, r_2 , and p_3) but we find that one general configuration works best. The first breakpoint r_1 occurs at a few hundred r_s , with $B(r) \rightarrow \text{constant}$ (i.e., $p_2 = 0$). Interestingly, the second breakpoint r_2 is at $\sim 3r_s$, the radius of the last

stable orbit for a non-rotating black hole. At that point, $B(r) \propto r^{-3-6}$, which suggests the presence of a magnetic dynamo at small radii.

These three segments of $B(r)$ (an equipartition region, a region of constant field intensity, and a dynamo region) are all necessary to fit the general flat spectral shape of Sgr A*. The equipartition region results in a sufficiently large field and temperature to reproduce the observed flux at low frequencies (i.e., $10^9 \lesssim \nu \lesssim 10^{10}$ Hz) with r large enough so that the emission is not self-absorbed. The region of constant magnetic field is required to match the flat spectral index of ~ 0.3 (Lo 1986) at moderate radio frequencies ($10^{10} \lesssim \nu \lesssim 10^{11}$ Hz). At $\sim 2 \times 10^{11}$ Hz there is an observed sub-millimeter excess, presumably due to an ultra-compact component a few r_s in size (Falcke et al. 1998); our dynamo region produces this excess. There are many arguments (see, e.g., Hawley & Balbus 1992) for the presence of a magnetic dynamo close to a black hole so such a component is not implausible.

The calculation of the magnetic bremsstrahlung contribution to j_ν assumes that μ , the cosine of the angle between the flow and the line of sight, is the same as the cosine of the angle between B and the line of sight. For a spherical flow, in the absence of magnetic reconnection (which should be minimal for $r \gg R_A$ anyway), $B_r \propto r^{-2}$, while $B_\theta \propto r^{-1}$. Thus, even if the magnetic field at infinity is perfectly tangled, it is reasonable to assume that at R_0 , $B_r \gg B_\theta$. However, because the magnetic field is divergence-less, the stretched out field lines must close somewhere. Presumably this occurs quite close to the black hole. In a fully self-consistent calculation, we will use the distributions derived from an actual 3D hydrodynamic simulation as the basis for calculating the emissivity.

4. Results

We present the resulting spectrum of our best fit model in Figure 1(a). For comparison with previous calculations (e.g., Melia 1994), we also plot results for a model which assumes only gravity acts to accelerate the accreting gas (i.e., $H \equiv 0$). Since the flow is only mildly supersonic at moderate radii, the assumption of free-fall is physically invalid, but such models do allow hotter gas to exist at larger radii and, thus, have more emission at lower frequencies than the full solution models. Nonetheless, both model spectra are consistent with the observations over 16 decades of frequency. The parameters used in the two fits are given in Table 1. Note that one clear prediction of these models is that the source of the majority of the high energy γ -ray emission is not Sgr A* or its associated accretion flow, unless some exotic particle acceleration mechanism is operating within the inflow. This is consistent with recent models (Melia, Yusef-Zadeh, & Fatuzzo 1998), which suggest the GC high energy emission is due to Sgr A East, a super-nova-like remnant near or possibly even enveloping Sgr A*. The details of the predicted emission in the IR region are fairly sensitive to the details of radiative transport, since the gas circularizes at small radii, possibly producing a small disk which emits primarily in the IR. Nonetheless, the next generation of infrared observations should be able to detect the emission from the inner $\sim 10r_s$ of the black hole.

Some of the observations used in Figure 1(a) are averaged over a span of years while others are contemporaneous. Since the flux of Sgr A* can vary with time by more than 25% (depending on frequency), we do not necessarily wish to reproduce the entire suite of observations but rather the general trend. The resolution of the observations also varies greatly but most of the values reported in the table have backgrounds subtracted out and in principle refer to the flux of Sgr A* only. Those observations which have a potential for source confusion are plotted as upper limits. For example, at $\nu \gtrsim 8.6 \times 10^{11}$ Hz, the

Table 1: Parameters for the Sgr A* Spectral Fits

Parameter	Full Solution	Free-fall
$\dot{M}_{\odot} \text{ yr}^{-1} (\text{gsec}^{-1})$	8×10^{21}	5×10^{21}
$v_{\infty} (\text{km s}^{-1})$	500	1000
f_R	1.0	1.0
f_T	0.5	1.0
f_v	0.5	1.0
η	0.05	0.15
p_1	2.5	2.5
p_2	0.0	0.0
p_3	6.0	12.0
$r_1(r_s)$	750	2000
$r_2(r_s)$	4	3

Model parameters for two fits to the spectrum of Sgr A*, assuming spherical accretion. The full solution is for a calculation using the equations described in the text while the free-fall model assumes $H \equiv 0$ so that only gravity accelerates the infalling gas (see Eq. [14]).

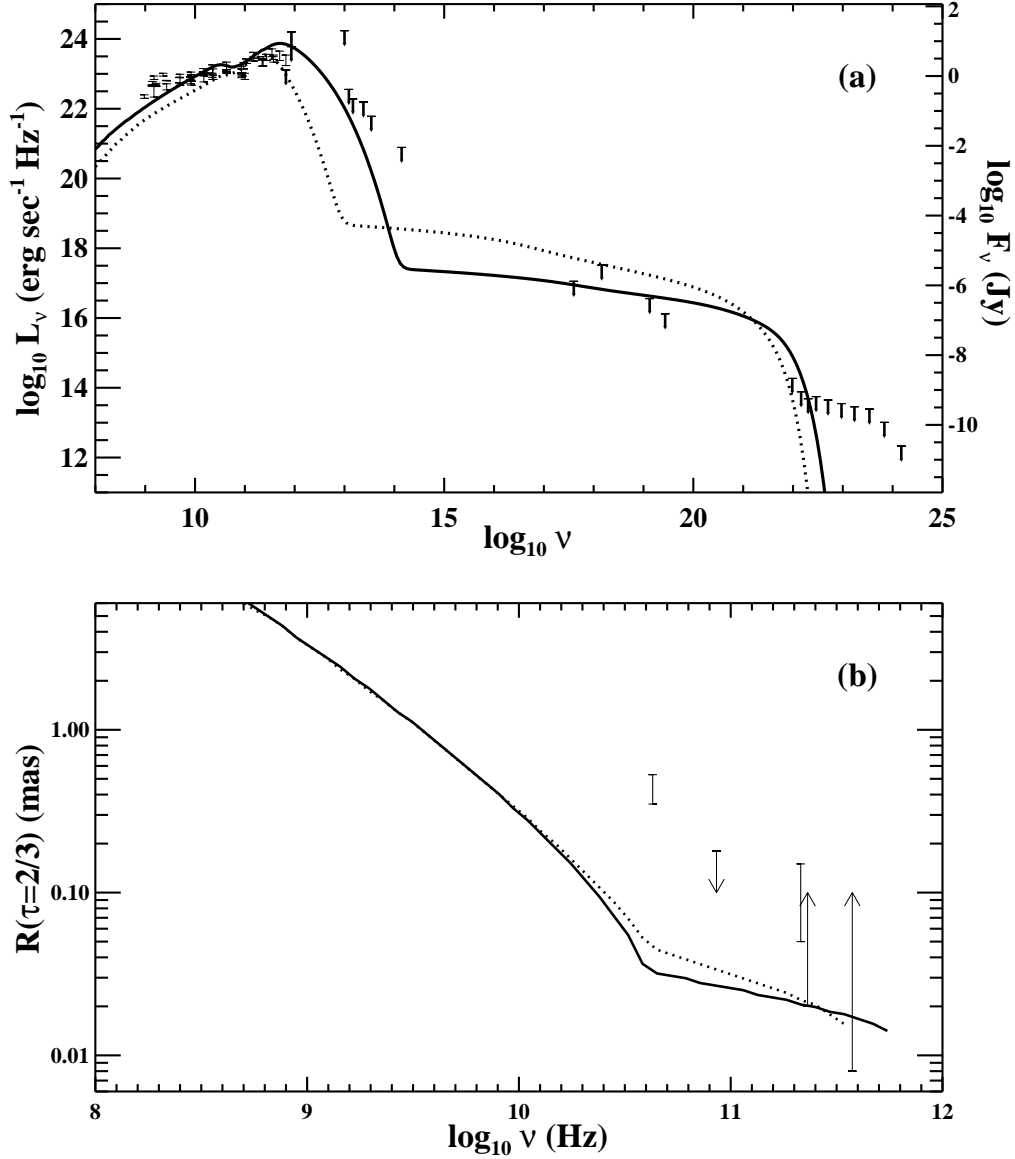


Fig. 1.— The solid curves are for a model which assumes pure free-fall ($H \equiv 0$) while the dotted curves are for a model which uses the complete equations (see text for details). (a) The observed spectrum of Sgr A* along with the predicted results for the best model fits. The observational data are taken from various sources (see Narayan et. al. 1998 for a recent compilation). (b) The observed size of Sgr A* along with the predicted size, defined as the radius at which the optical depth, $\tau_{\nu_0}^\infty(r)$ equals 2/3.

background emission due to, e.g., dust at a temperature of 90K, is comparable to emission from Sgr A* itself (Zylka et al. 1992). This is particularly true in the infrared, where Sgr A* has yet to be definitely identified and has a flux considerably less than that of the surrounding gas and stars, and in the X-rays and γ -rays, where the poor spatial resolution is likely to result in multiple sources being in the field of view. Similarly, observations at $\nu \lesssim 1$ GHz are unreliable as limits for the luminosity of Sgr A* due to source confusion, scattering, and self-absorption (Davies et al. 1976). In converting the observed fluxes to the luminosities plotted in Figure 1(a), it is assumed that Sgr A* is 8.5 kpc away.

The predicted size of Sgr A* is shown in Figure 1(b). Also shown are the present observational limits and measurements (see Lo et al. 1998 for a summary of recent work). At present there are two observations which address the intrinsic diameter of the minor axis of Sgr A*. However, these observations are difficult and, for example, may have had difficulties with calibration (see, e.g., Krichbaum et al. 1998). The model satisfies the upper limit at 3.5mm as well as the lower limit at 0.8mm, but it predicts a source that is somewhat more compact than the other observations suggest. But while the observations tend to fit Gaussian FWHM to the data, the predicted diameter is defined as the last scattering surface (i.e., $r[\tau = 2/3]$). For a more detailed and accurate size comparison, one needs a more sophisticated treatment, using, for example, the theory of wave propagation in an extended, irregular medium (Melia, Jokiipii & Narayanan 1992). In addition, at small radii, the presence of angular momentum and asymmetries in the flow will result in a distended non-circular source shape. For example, at 7mm the axial ratio is observed to be less than 0.3 (Lo et al. 1998). Thus, the model size results presented here should be taken as approximate lower limits.

In Figure 2 we show the radial profiles for the temperature and magnetic field for the two fits shown in Figure 1. The gas is always sub-virial ($T_{vir} \sim 10^{12}$ K $[r/r_s]^{-1}$) with

a peak temperature of $\sim 10^{11}\text{K}$. This peak temperature is within the present observed lower ($1.3 \times 10^{10}\text{K}$; Lo et al. 1998) and upper ($5 \times 10^{11}\text{K}$; Gwinn et al. 1991) brightness temperature limits. Only within $\sim 10^{2-3}r_s$ of the black hole, where the gas becomes relativistic, is there significant magnetic bremsstrahlung emission. It is not a coincidence that r_1 is $\sim 10^3r_s$. The accreting gas must stay hot enough at such radii to produce the flat spectrum; the constant magnetic field and subsequent heating via reconnection very nearly achieve this. However, this cannot continue all the way down to the event horizon or else the resulting magnetic field is insufficient to produce the observed sub-millimeter excess and the gas gets too hot to continue accreting and becomes pressure supported. Thus, we require a sharp increase in the magnetic field strength within $\sim 10r_s$ of the black hole with a resulting peak magnetic field of ~ 100 Gauss. We postulate that this may occur when the frozen-in magnetic field lines, which have been stretched out during the accretion process, finally close or are twisted by sheared gas motions due to a transition resulting from residual angular momentum in the flow; however, if the viscosity is large, the bulk gas flow still remains primarily radial and supersonic (Narayan et al. 1997). As described by Hawley and Balbus (1992), instabilities in the flow, possibly tied to differential rotation once the gas circularizes, may result in the generation of strong poloidal and toroidal fields, driving the magnetic field strength up to thermal equipartition, as required in our model. Except in the transrelativistic region ($\sim 10^3r_s$), the gas density and velocity profiles are close to that from free-fall so that $n \sim 10^{10}(r_s/r)^{3/2}\text{cm}^{-3}$.

5. Conclusions

By incorporating an enhanced treatment of the magnetic bremsstrahlung emissivity and solving the accretion flow equations explicitly, we have improved the accreting black hole model for Sgr A* with resulting spectra that are consistent with observations over more

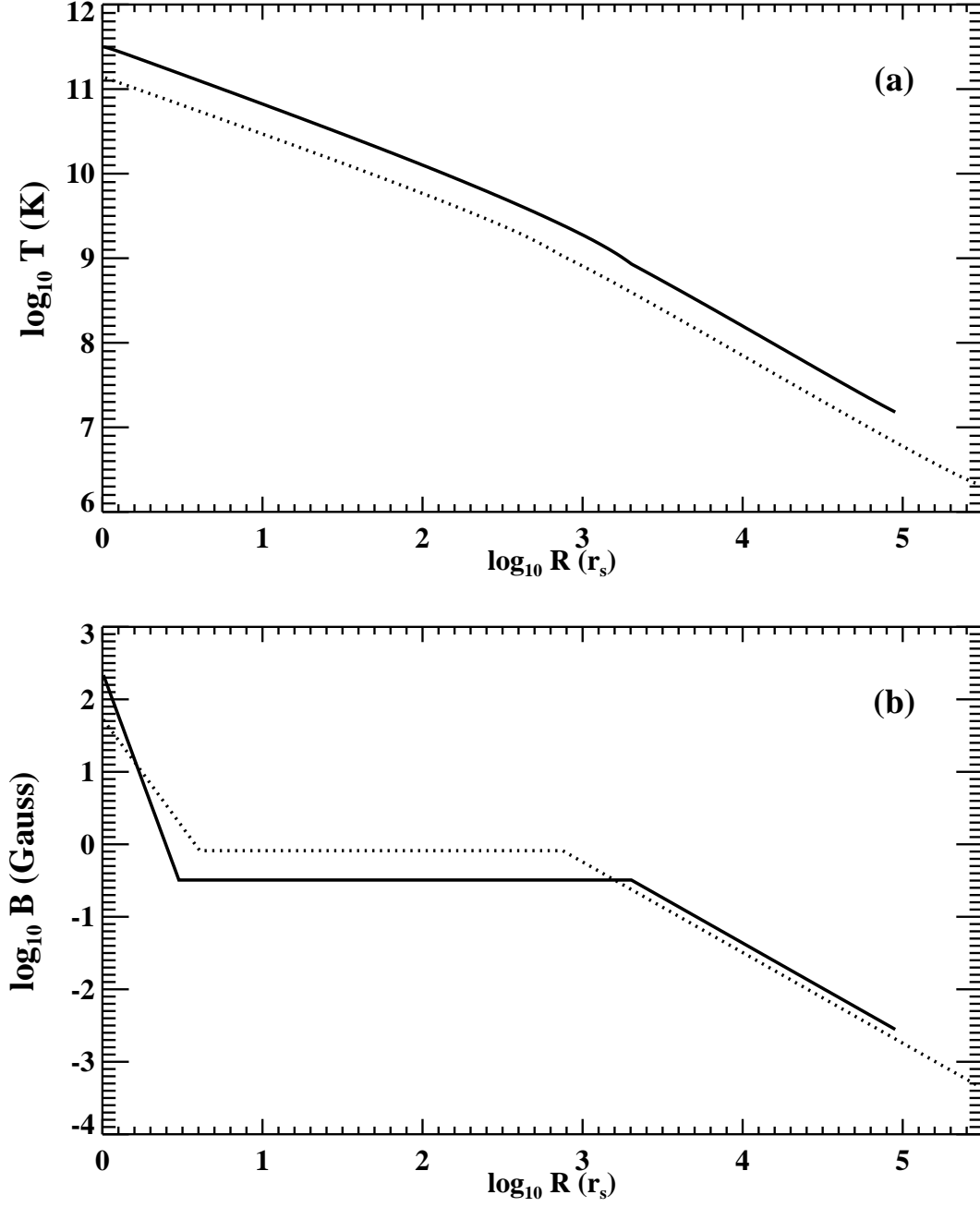


Fig. 2.— Plots of temperature (a) and magnetic field (b) versus radius for the two best fit models. The solid curves are for a model which assumes pure free-fall ($H \equiv 0$) while the dotted curves are for a model which uses the complete equations (see text for details).

than 16 decades of frequency. The mass accretion rate of $\sim 10^{-4} M_{\odot}\text{yr}^{-1}$, as determined from the spherical accretion model, is consistent with the rate expected on the basis of observations and hydrodynamical arguments (see, e.g, Coker & Melia 1997). However, other models, such as an “advection dominated accretion flow” (ADAF) with outflow (Blandford & Begelman 1999), require an accretion rate that is 2 or more orders of magnitude smaller than this.

There are some difficulties with the model. The full solution, using the Euler equation, suggests that the flow may be transonic and that it may therefore shock at smaller radii. A shock could produce high energy particles, which would result in significant magnetic bremsstrahlung emission at larger radii (Markoff, Melia, & Sarcevic 1997), thereby increasing the emission at lower frequencies. We hope to address this difficulty in future work. It is interesting that the break seen in the low energy γ -ray observations coincides with the high energy turnover in the model, suggesting the presence of another, hotter source within the field of view of EGRET. In addition, we have effectively ignored the role played by angular momentum, the presence of which would introduce viscous processes that are even more poorly understood than magnetic reconnection. Also, the handling of radiative transport has so far been very simplistic. Inclusion of relativistic 3D radiative transfer, including ray bending and inverse Compton, could potentially alter the resulting spectra significantly.

The model suggests that if the accretion rate onto Sgr A* is large ($\sim 10^{-4} M_{\odot}\text{yr}^{-1}$) then the observed X-ray emission from the GC is due to the extended X-ray emission from this accretion process. However, the observations have a resolution on the order of arcminutes while the ‘extended’ emission region from the model spans a few arcseconds. Due to calibration difficulties and an uncertain column depth between here and the GC, the observed X-ray limits are uncertain to within a factor of a few (Narayan et al. 1998) so

the model is still marginally consistent with the X-ray observations. The next generation of observations (such as with Chandra) will most likely settle this issue.

The picture with which we have worked here under-predicts somewhat the low frequency radio emission. Within the context of the model, unreasonable temperature and magnetic field profiles are required to fit the observations and even then the fit at other frequencies degrades. This difficulty is due to two things. First, the low frequency emission from close to the black hole is trapped so it does not contribute to the low frequency spectrum. Second, gas with sufficient magnetization and temperature to produce the observed magnetic bremsstrahlung emission at large radii is gravitationally unbound and could not self-consistently accrete. An improvement to the model that addresses this low- ν deficiency in the spectrum may come with more realistic 3D simulations, which will be reported elsewhere.

Finally, although we have briefly touched on the likely importance of the sub-millimeter excess to our understanding of the environment just outside the event horizon, this clearly is an issue that warrants further detailed theoretical work. Taking into account scatter-broadening of the image in the interstellar medium, and the finite achievable telescope resolution, the $\sim 10r_s$ “shadow” of the Galactic Center black hole (see, e.g., Falcke, Melia & Agol 1999) should be well observable with very long-baseline interferometry at sub-millimeter wavelengths. In our picture, the dynamo effect that leads to the intensification of the magnetic field that accounts for this spectral excess may be due to the circularization of the infalling gas when it approaches the circularization radius $2\lambda^2 r_s$ (see § 3.1). We are in the process of examining the behavior of the magnetized plasma when shearing motions become important in this region, and we will report on the results of this investigation in the near future.

REFERENCES

- Allen, D., Hyland, A., & Hillier, D. 1990, MNRAS, 244, 706.
- Beckert, T., Duschl, W.J., Mezger, P.G., & Zylka, R. 1996, AA, 307, 450.
- Beckert, T. & Duschl, W.J., 1997, AA, 328, 95.
- Bower, G.C. & Backer, D.C. 1998, ApJ Letters, 496, 97L.
- Coker, R.F. & Melia, F. 1997, ApJ Letters, 488, L149.
- Coker, R.F. & Melia, F. 1999, ApJ, submitted.
- Eckart, A. & Genzel, R. 1996, Nature, 383, 415.
- Eckart, A. & Genzel, R. 1999, in The Central Parsecs: Galactic Center Workshop 1998 (ASP: San Francisco).
- Falcke, H., Mannheim, K., Biermann, P.L. 1993, AA, 278, L1.
- Falcke, H., Goss, W.M., Matsuo, H., Teuben, P., Zhao, J., & Zylka, R. 1998, ApJ, 499, 731.
- Falcke, H., & Biermann, P.L. 1999, AA, 342, 49.
- Falcke, H., Melia, F., & Agol, E. 1999, ApJ Letters, submitted.
- Geballe, T., Krisciunas, K., Bailey, J., & Wade, R. 1991, ApJ Letters, 370, L73.
- Genzel, R. 1998, BAAS, 193, 62.01.
- Genzel, R., et al. 1996, ApJ, 472, 153.
- Genzel, R., Eckart, A., Ott, T. & Eisenhauer, F. 1997, MNRAS, 291, 219.
- Ghez, A.M., Klein, B.L., Morris, M., & Becklin, E.E. 1998, ApJ, 509, 678.

- Hall, D., Kleinmann, S., & Scoville, N. 1982, *ApJ Letters*, 260, L53.
- Haller, J.M., et al. 1996, *ApJ*, 456, 194.
- Hanson, M.M., Rieke, G.H., & Tamblyn, P. 1998, *BAAS*, 193, 104.02.
- Hawley, J.F. & Balbus, S.A. 1992, *ApJ*, 400, 595.
- Ipsier, J.R. & Price, R.H. 1977, *ApJ*, 216, 578.
- Ipsier, J.R. & Price, R.H. 1982, *ApJ*, 255, 654.
- Jackson, J.M., et al. 1993, *ApJ*, 402, 173.
- Kowalenko, V. & Melia, F. 1999, *MNRAS*, in press.
- Krabbe, A., Genzel, R., Drapatz, S., & Rotaciuc, V. 1991, *ApJ Letters*, 382, L19.
- Lang, K. 1980, *Astrophysical Formulae* (Springer-Verlag: New York).
- Lo, K.Y. 1986, *PASP*, 98, 179L.
- Mahadevan, R., Narayan, R. & Yi, I. 1996, *ApJ*, 465, 327.
- Marshall, J., Lasenby, A.N. & Yusef-Zadeh, F. 1995, *MNRAS*, 274, 519.
- Melia, F. 1988, *JCoPh*, 74, 488.
- Melia, F. 1992, *ApJ Letters*, 387, L25.
- Melia, F. 1994, *ApJ*, 426, 577.
- Melia, F. & Coker, R. 1999, *ApJ*, 511, 750.
- Melia, F., Jokipii, J.R., & Narayanan, A. 1992, *ApJ Letters*, 395, L87.

- Najarro, R., Krabbe, A., Genzel, R., Lutz, D., Kudritzki, R., & Hillier, D. 1997, AA, 325, 700.
- Narayan, R., Yi I., & Mahadevan, R. 1995, Nature, 374, 623.
- Narayan, R., Mahadevan, R. et al. 1998, ApJ, 492, 554.
- Ozernoy, L. 1989, in The Center of the Galaxy, ed. M. Morris (Kluwer: Dordrecht), p. 555.
- Parker, E.N. 1960, ApJ, 132, 175.
- Petschek, H.E. 1964, Proc. of the Symposium on Physics of Solar Flares (NASA SP-50), 425.
- Ruffert, M. & Melia, F. 1994, *A.A.Letters*, 288, L29.
- Rybicki, G. & Lightman, A. 1979, Radiative Processes in Astrophysics (Wiley and Sons: New York).
- Shapiro, S.L. 1973, ApJ, 185, 69.
- Shapiro, S. & Teukolsky, S. 1983, Black Holes, White Dwarfs, and Neutron Stars (New York: Wiley and Sons).
- Tamblyn, P., Rieke, G.H., Hanson, M.M., Close, L.M., McCarthy, D.W. Jr. & Rieke, M.J. 1996, ApJ, 456, 206.
- van Hoven, G. 1979, ApJ, 232, 572.
- Xu, G. & Chen, X. 1997, A.A.Letters, 489, L29.
- Yusef-Zadeh, F. & Melia, F. 1991, ApJ Letters, 385, L41.
- Yusef-Zadeh, F., Roberts, D.A., Goss, W.M., Frail, D., & Green A. 1996, ApJL, 466, L25.

Zel'dovich, Y.B. & Novikov, I.D. 1971, *Relativistic Astrophysics* (University of Chicago: Chicago).

Zylka, R., Mezger, P.G., Ward-Thomson, D., Duschl, W. & Lesch, H. 1995, *AA*, 297, 83.